

Synthesis of Glue-Free NaA Zeolite Granules from Natural Kaolin for the Adsorption of Pb(II) Ions in Aqueous Solution Using a Fixed-Bed Column Study

Hieu Nguyen Phuoc, Quang Thanh Le, Tung Cao-Thanh Pham,* and Thanh Tu Le*



Cite This: *ACS Omega* 2021, 6, 21024–21032



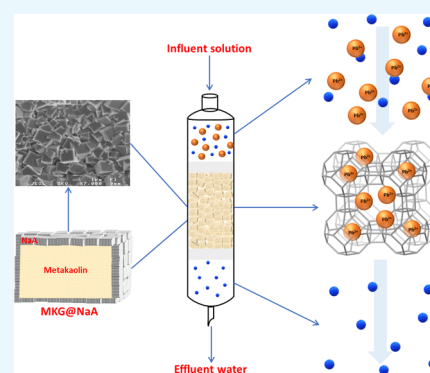
Read Online

ACCESS |

Metrics & More

Article Recommendations

ABSTRACT: NaA zeolite-coated metakaolin granules (MKG@NaA) were successfully synthesized from kaolin mineral by primary growth in the hydrothermal reaction without using glue or a seed crystal. The XRD and SEM analysis results revealed that a layer of NaA zeolite with a typical cubic shape and high crystallinity formed on the surface of kaolin granules. The obtained material was used as an adsorbent for lead metal ion Pb(II) adsorption studies in a fixed-bed column configuration. The operation factors such as the solution inflow rate, Pb(II) concentration, and column height were investigated. The results showed that the adsorption capacity of the material increased with increasing column height and initial concentration of the influent and decreased with increasing flow rate. With the test parameters at the Pb(II) concentration of 100 mg·L⁻¹, the adsorbent bed height of 8.1 cm, and the inflow rate of 2.5 mL·min⁻¹, the lead ion adsorption capacity was 118.5 mg·g⁻¹. The Thomas, Yoon–Nelson, and bed depth service time models were applied to describe the breakthrough curves for Pb(II) ion removal by a fixed-bed column using the MKG@NaA adsorbent and to predict the column performance under different experimental conditions with good linearity ($R^2 > 0.95$).



1. INTRODUCTION

Zeolites are microporous crystalline aluminosilicates with a three-dimensional open framework structure. They are composed of alumina and silica tetrahedron-forming regular interconnected pores and channels. Due to the presence of mixed oxide in the composition, the negative charge exists in the framework and creates properties of zeolite that are more useful compared to other amorphous porous materials. The negative charge centers are often neutralized by cations such as Na⁺, K⁺, and Ca²⁺, which would be eventually exchangeable with certain heavy metal ions in solutions.¹ Depending on the framework type and composition of zeolites, their microstructure property could vary from hydrophilic to highly hydrophobic and show outstanding behaviors in adsorption application such as high selectivity to radioactive Cs and Sr metal ions or radioactive iodine and methyl iodide molecules.^{2–5} Of a large number of synthetic zeolites, Linda Type A (LTA) zeolite has the lowest silicon/aluminum (Si/Al) ratio of 1:2, leading to the highest cation exchange capacity.^{1,6} LTA zeolite is one of the most common zeolites used to remove heavy metal and radioactive metal ions from aqueous solution.^{7–11} Several approaches have been applied to synthesize LTA zeolite such as using pure chemicals, fly ash, silicate minerals, and kaolin minerals.^{8,9,12,13} Among the natural material sources for LTA zeolite synthesis, kaolinite is the most popular precursor due to its low cost, abundance,

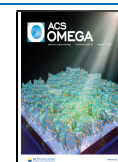
and similar Si/Al ratio to LTA zeolite.^{13,14} However, to be used for LTA zeolite preparation, kaolin has to be calcined to turn to amorphous metakaolin form. Depending on the original source, kaolin materials may contain impurities that affect the quality and property of zeolite products such as iron oxide, manganese oxide, or titanium oxide.^{15,16} There was another route to utilize natural kaolin for zeolite synthesis without activation by calcination. However, it required multistep treatment by soaking and heat treatment in NaOH solution, dissolving in dilute HCl acid, and re-neutralizing to collect amorphous Si–Al gel prior to converting to zeolite.^{17,18}

In most cases, the LTA zeolite was obtained in powder form, which has limited usage, especially in adsorption–recovery and regeneration processes. In addition, zeolite in powder form is not suitable for dynamic adsorption, as the small size of a zeolite particle leads to aggregation and leakage during the column adsorption process, hindering its application in dynamic adsorption in practice.^{19,20} Several techniques have been studied to immobilize or fabricate granules containing

Received: May 20, 2021

Accepted: July 27, 2021

Published: August 6, 2021



zeolite powder. Yan's group recently reported the synthesis of LTA monolith by combining casting and calcination processes using kaolin paste and polymer beads as a template.²¹ The composite adsorbent was prepared by attaching magnetic metal oxide to the zeolite particle to increase the ability to separate and collect the adsorbent by applying a magnetic force.^{9,22}

Adsorption studies are classified into static and dynamic adsorption processes.²³ In laboratory-scale metal ion adsorption studies, they are often done in batch form due to the simple conduction. However, in the industrial scale, the batch experiment is ineffective because the parameters obtained from the static condition test are not suitable in the case where dynamic adsorption is not at equilibrium.^{23–25} The parameters obtained from the laboratory scale using column adsorption configuration are closer to practical operation conditions and can be used on the industrial scale for adsorption and heavy metal removal in continuous flow systems.

Heavy metals are among the most crucial water pollutants and are becoming one of the most serious environmental problems globally. Heavy metals are highly toxic and hazardous, affecting human health and ecosystems. They are not decomposable through chemical and biological processes in the environment and tend to bioaccumulate.²⁶ For instance, lead metal ions are one of the popular heavy metals of concern in environmental pollution. It can enter the environment through oil refining, mining works, paint, electroplating, metal production industry, textile dyeing, wood preservation, battery production, agricultural activities and urban wastewaters, and glass industries.^{26–28} As one of the most hazardous heavy metal pollutants listed by the United States Environmental Protection Agency (USEPA), Pb(II) can cause critical illnesses including central nervous system damage, hypertension, kidney cancer, brain dysfunction, basic cellular processes disorders, teratogenic effects, and diseases affecting the liver, circulatory system, and reproductive system.^{28,29} Hence, developing an efficient method for removal of Pb(II) metal ions is of great importance from both environmental and human health points of view.

There are several materials and techniques that are being used to remove heavy metal ions from solutions, including solid-phase extraction, solvent extraction, membrane filtration, chemical precipitation, electrodialysis, reverse osmosis, adsorption, and ion exchange. Among these methods, adsorption is one of the most efficient methods due to its low cost and simple operation.^{30,31} As one of the alternatives, zeolites are considered to be adsorbents for heavy metal treatment due to their large surface area, good ion exchange capacities, hydrophilicity, eco-friendliness, low cost, and easily tunable chemical characteristic.^{27,28}

In this work, we report the synthesis of NaA zeolite coated on metakaolin granules (MKG@NaA) and used it as an adsorbent for filtration and removal of Pb(II) ions in aqueous solution using a fixed-bed column operation process. Zeolite crystals grew on the surface of 2–3 mm kaolin granules by simple hydrothermal treatment of pristine granular metakaolin in NaOH solution without adding additional zeolite seed crystals. The removal of Pb(II) metal ions in a fixed-bed column configuration was conducted and studied with various operational parameters including the solution flow rate, initial Pb(II) ion concentration, and height of the bed layer. The Thomas model, Yoon–Nelson model, and bed depth service

time (BDST) model were applied to analyze the adsorption process.

2. RESULTS AND DISCUSSION

2.1. Characterization of Synthesized NaA Zeolite Crystals Coated on Metakaolin Granules.

We first prepared the porous granules as support for zeolite growth using natural kaolinite clay as described in detail in Section 4, and their characteristics are shown in Figure 1. The particle

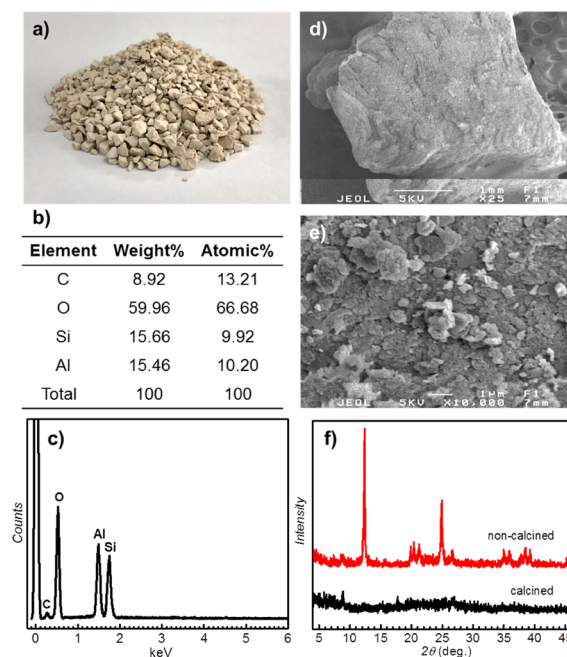


Figure 1. Characterization of kaolin material with a digital camera image of kaolin granules (a), EDX analysis results (b, c), SEM images with different magnifications (d, e), and XRD patterns of kaolin (noncalcined) and metakaolin (calcined) as indicated (f).

size and shape and element composition of kaolinite clay are presented in Figure 1a–c, respectively. The EDX result revealed that clay mainly contained silicon oxide (SiO_2) and aluminum oxide (Al_2O_3) with a Si/Al atom ratio of 0.97. The SEM images of granules showed a relatively rough surface containing a typical plate-like shape of kaolinite particles with the size of about $1 \mu\text{m}$ (Figure 1d,e). It is known that the typical crystalline structure of kaolinite clay would completely collapse and turn to metakaolin form after heat treatment at high temperatures. In this work, the kaolinite granules were treated at 500°C for 3 h, and their XRD pattern in Figure 1f confirmed that the amorphous metakaolin was the component that existed in the granules.

In this work, the metakaolin used as a starting material was composed of silicon and aluminum oxides with a Si/Al atom ratio of 0.97. It was ideal for the synthesis of highly aluminum-contained zeolite without adding any additional aluminum or silicon source. We conducted the hydrothermal reaction with a reactant mixture prepared by simply soaking metakaolin granules in a NaOH aqueous solution. We observed that the typical cubic-shaped NaA zeolite formed on the surface of the kaolin granule after 24 h of reaction period (Figure 2a). With increasing reaction time, the size of zeolite crystals increased, and the impurity phase was also observed as shown in SEM images in Figure 2b,c. However, with the additional aging

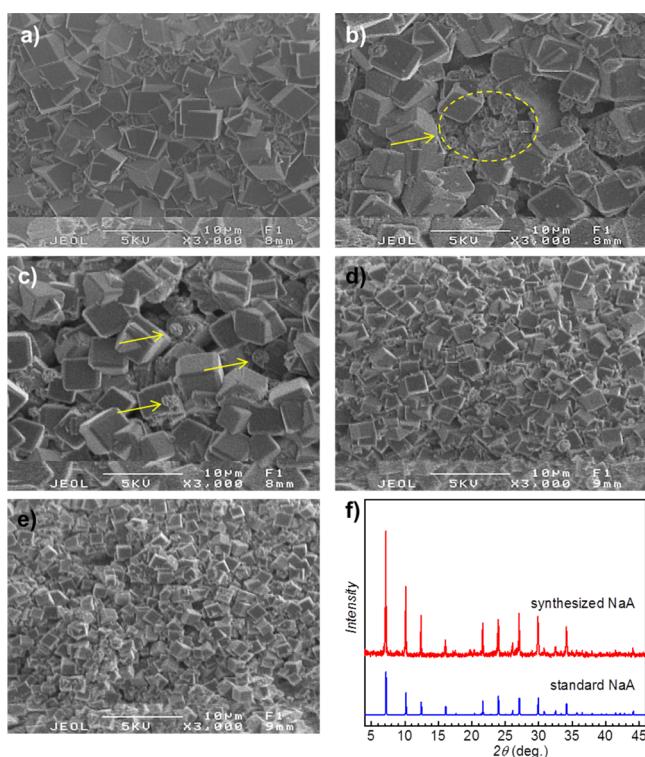


Figure 2. SEM images of NaA zeolite coated on granular kaolin MKG@NaA obtained from hydrothermal reaction for 24 h (a), 48 h (b), and 72 h (c) from the reaction mixture without aging, hydrothermal reaction for 24 h with reaction mixtures aged for 24 h under static conditions (d) and with 200 rpm stirring (e), and XRD pattern of obtained NaA (f).

condition, the pure phase of NaA zeolite was obtained. The pure NaA zeolite, as shown by the SEM image in Figure 2d, was produced from the reaction mixture of kaolin granules and NaOH solution that had been aged for 24 h under static conditions. A similar product was obtained from a reaction mixture that was aged for 24 h and gently stirred at 200 rpm (Figure 2e). The XRD pattern in Figure 2f confirmed that the highly crystalline and pure phase of NaA zeolite was obtained in this synthesis condition.

The SEM image in Figure 3 revealed that a layer of NaA zeolite containing crystals with an average size of $1.4 \mu\text{m}^3$ formed on the outer surface of the kaolin granule (Figure 3a,b). Cross-sectional view SEM images showed the zeolite layer with the thickness of about $2 \mu\text{m}$ covering the outer surface of the granule (Figure 3c), and individual particles formed in some voids inside the kaolin granule (Figure 3d). The calculated value of the NaA zeolite amount contained in the MKG@NaA adsorbent was 1.62%. The EDX analysis results obtained from MKG@NaA showed the NaA zeolite layer with a Si/Al ratio of 1.1 and sodium (Na) as a counter-cation covering the surface of kaolin granules (Figure 3e,f). This result revealed that there was a rearrangement of Si and Al atoms in the metakaolin material to form a new zeolite framework. Basically, in hydrothermal reaction conditions, metakaolin converts to zeolite in the presence of a basic solution such as NaOH.^{15,16} In this work, we observed that NaA zeolite formed a layer fully covering the surface of the metakaolin granule. This might result from the fact that NaOH can only interact with the outer surface of kaolin granules. Since these granules have a high bulk density, the NaOH

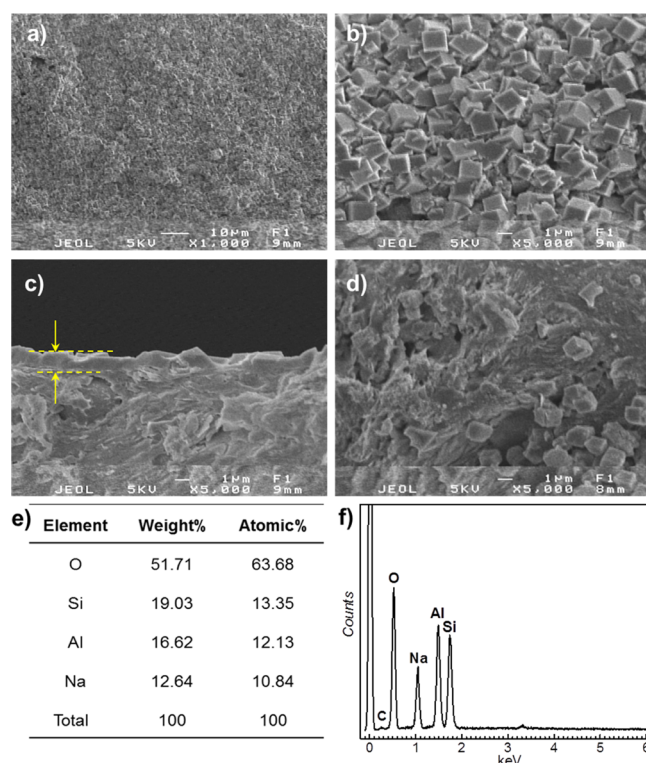


Figure 3. SEM images with different magnifications showing the top (a, b) and cross-sectional views (c, d) and EDX analysis results (e, f) of NaA zeolite synthesized on granular metakaolin.

solution cannot penetrate deeper into them; thus, NaA zeolite only forms on the outside.

2.2. Influence of Inflow Rate in the Dynamic Adsorption Experiment. We first carried out the heavy metal removal experiment using a batch reactor and NaA zeolite powder adsorbent. The experiment results showed that among metal ions including Pb(II), Cd(II), Co(II), and Ni(II), NaA zeolite quickly adsorbed with high removal efficiency to Pb(II) and Cd(II), while the removal efficiency of NaA zeolite was relatively lower for Co(II) and Ni(II) ions under the same experiment conditions (Figure 4a). In all cases, the adsorption capacity of NaA zeolite to study metal ions increased with increasing initial concentration. The highest adsorption capacity of NaA zeolite to Pb(II) in this experiment was obtained at $560 \text{ mg}\cdot\text{g}^{-1}$ with an initial concentration of Pb(II) ion in solution of $450 \text{ mg}\cdot\text{L}^{-1}$. With a further increase in Pb(II) concentration in solution, the adsorption of NaA zeolite powder saturated and the adsorption capacity was not changed. These values were higher compared to those obtained in the Cd(II) ion case. The adsorption capacity and initial concentration of Cd(II) were $250 \text{ mg}\cdot\text{g}^{-1}$ and $600 \text{ mg}\cdot\text{L}^{-1}$, respectively (Figure 4b). The experiment resulted in heavy metal adsorption using NaA zeolite powder, and the batch reactor showed that NaA zeolite has high affinity and adsorption capacity to Pb(II) ions.

Taking advantage of this result, we conducted the dynamic adsorption experiment using a fixed-bed column with an MKG@NaA adsorbent and Pb(II) single ion solution. The crucial parameter in dynamic adsorption systems is the inflow rate, particularly in industrial utilization. The breakthrough curves for the adsorption of Pb(II) using MKG@NaA at inflow rates of 2.0, 2.5, and $3.0 \text{ mL}\cdot\text{min}^{-1}$ are shown in Figure 5a. The

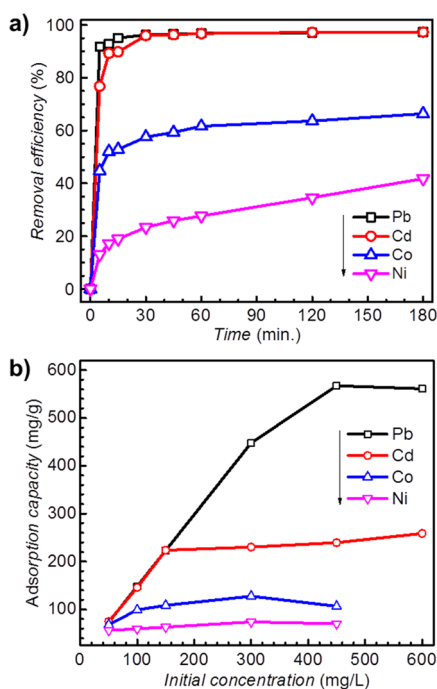


Figure 4. Plot of removal efficiency of NaA zeolite powder with respect to operation time in the removal of heavy metal ions as indicated (a) and plot of adsorption capacity of NaA zeolite powder to heavy metal ions including Pb(II), Cd(II), Co(II), and Ni(II) conducted in different initial concentrations of metal ions (b).

obtained result showed that with increasing flow rate from 2.0 to 3.0 mL·min⁻¹, the breakthrough curves became steeper and shifted toward a lower timescale. It was known that the flow rate is proportional to the Reynolds number and the mass transfer zone. However, it is inversely proportional to the breakthrough time and diffusion coefficient.³² As shown in Table 1, when the inflow rate ranged from 2.0 to 3.0 mL·min⁻¹, the adsorption capacity of Pb(II) varied from 115.0 to 90.4 mg·g⁻¹ and the saturation time decreased from 87 to 66 h. Obviously, the increase in flow rate led to reducing breakthrough points and saturation times. This result was due to Pb(II) ions having insufficient time to diffuse from the solution onto the zeolite pores and be captured by the adsorption sites inside the adsorbent.³² As a result, the removal efficiency of the column to Pb(II) was relatively low at high flow rates. In this work, we chose the flow rate of 2.0 mL·min⁻¹ for later studies.

2.3. Influence of Ion Concentration. The impact of the influent concentration on the adsorption behavior of a fixed-bed column was conducted with the Pb(II) concentration varying in values of 50, 80, and 100 mg·L⁻¹, a bed height of 8.1 cm, and a flow rate of 2.0 mL·min⁻¹. The breakthrough curves in Figure 5b with a typical S-shape indicated that the adsorbent absorbed and saturated quickly with the high concentration of Pb(II) ions in the solution. They also revealed that the saturation rate of the adsorbent and the breakout time of the bed column depended on the initial concentration Pb(II) ion, and the inlet concentration affected the diffusion process. Gouran-Orimi et al. reported that the higher concentration difference of solute in between the liquid and solid phases would increase the diffusion coefficient of Pb(II) and create more expeditious penetration of the liquid phase into the solid phase. As a result, the breakthrough time became shorter.³³

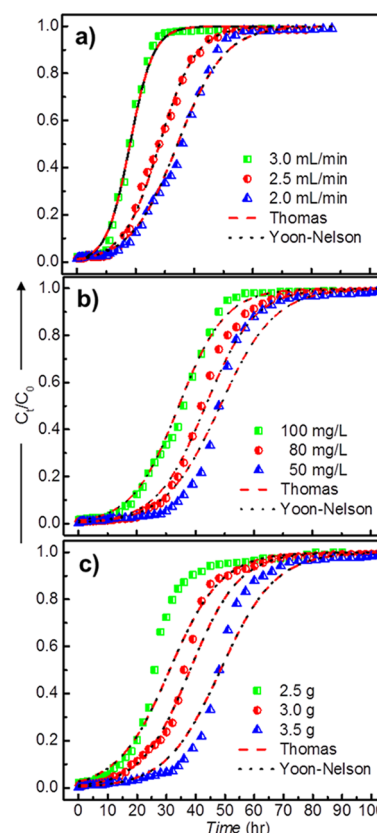


Figure 5. Breakthrough curves of fixed-bed column adsorption for the removal of Pb(II) ions using the MKG@NaA adsorbent conducted at different operation parameters by varying the solution inflow rate (a), Pb(II) concentration (b), and adsorbent amount or bed height (c); the solid block lines represent experimental data, the dashed line represents the Thomas model, and the dotted line represents the Yoon–Nelson model.

Additionally, Mokgehle et al. reported that at high metal concentrations, it created a driving power to scatter the metal ions into the water film, coating the adsorbent.²³

With the increase in Pb(II) concentration from 50 to 100 mg·L⁻¹, the 5% saturation point of the column shifted from 30 to 10 h, respectively (Figure 5b), the adsorption capacity of the column to Pb(II) increased from 80.9 to 115.0 mg·g⁻¹, and the saturation time decreased from 120 to 87 h as presented in Table 1. When the concentration increased, there was the concentration difference of Pb(II) ions in between the inflow solution and the water layer surrounding the fresh adsorbent particles. It created the concentration gradient and driving force that increased the diffusion rate of Pb(II) ions to the adsorbent surface. As a result, the bed column saturated faster.

2.4. Influence of the Fixed-Bed Height. It has been reported that the fixed-bed height column or the adsorbent amount strongly affected the adsorption process. In this work, the effect of fixed-bed height was investigated using columns packed with MKG@NaA at three different bed heights of 5.8, 6.9, and 8.1 cm, which corresponded to 2.5, 3.0, and 3.5 g of MKG@NaA, respectively. The experiments were conducted at a flow rate of 2.0 mL·min⁻¹ and an influent concentration of 50 mg·L⁻¹. The obtained result in Figure 5c showed that the breakthrough time of Pb(II) adsorption was delayed and the breakthrough curves gradually increased with increasing bed height. The breakthrough time of Pb(II) adsorption at C_t/C₀

Table 1. Column Performance Result Obtained from Experiment and Calculated Data Using the Thomas Model and Yoon–Nelson Model in Removal of Pb(II) Ions by Fixed-Bed Column Filtration and MKG@NaA Adsorbent^a

experimental conditions			experimental parameters of breakthrough curves				Thomas model			Yoon–Nelson model		
<i>m</i> (g)	<i>C</i> ₀ (mg/L)	<i>Q</i> (mL/min)	τ_{exp} (h)	<i>t</i> _s (h)	<i>q</i> _e (mg/g)	<i>R</i> _{total} (%)	<i>k</i> _{Th} (mL/mg·min)	<i>q</i> ₀ (mg/g)	<i>R</i> ²	<i>k</i> _{YN} (min)	τ (h)	<i>R</i> ²
2.5	50	2.0	26	90	62.6	11.60	0.038	74.6	0.9512	0.0019	31.08	0.9512
3.0	50	2.0	36	106	70.0	11.01	0.040	76.1	0.9874	0.0020	38.06	0.9874
3.5	50	2.0	48	120	80.9	11.23	0.036	83.1	0.9749	0.0018	48.46	0.9749
3.5	80	2.0	42	110	114.2	10.81	0.025	119.2	0.9843	0.0020	43.47	0.9843
3.5	100	2.0	36	87	115.0	10.65	0.021	117.6	0.9802	0.0021	34.30	0.9802
3.5	100	2.5	28	78	118.5	12.66	0.027	120.7	0.9856	0.0027	28.15	0.9856
3.5	100	3.0	18	66	90.4	11.41	0.042	92.9	0.9694	0.0042	18.06	0.9694

^a*m*, weight of the adsorbent (g); *C*₀, influent concentration (mg/L); *Q*, flow rate (mL/min); *t*_s, saturation time (h); *q*_e, equilibrium column capacity (mg/g); *R*_{total}, total removal percent of Pb(II) (%); *k*_{Th}, Thomas rate constant (mL/mg·min); *q*₀, adsorption capacity (mg/g); *k*_{YN}, Yoon–Nelson rate constant (min); τ_{exp} , time required for 50% adsorbate breakthrough (h).

of 0.05 increased from 10 to 35 h, with increasing packing heights of the adsorbent from 5.8 to 8.1 cm, respectively. Additionally, the obtained results in Table 1 revealed that when the packing weight of the adsorbent in the bed increased from 2.5 to 3.5 g, the adsorption capacity of the column increased from 62.6 to 80.9 mg·g⁻¹, and the saturation time increased from 90 to 120 h, respectively. Generally, the more adsorbent packed or the more column height increased, the higher the adsorption capacity of the column obtained. This occurred because the increasing bed height provides a larger surface area and more exchangeable sites available for Pb(II) ions to be absorbed. Furthermore, the increase in adsorbent amount provided a greater contact time between lead ions and the fixed-bed column, thus providing better intraparticle phenomena as observed in other works.^{23,24,33}

2.5. Adsorption Models. **2.5.1. Thomas Model.** The Thomas model is one of the most widely used models to describe column adsorption data in dynamic adsorption experiments at different fixed-bed heights, inflow rates, and influent concentrations. This model assumes Langmuir kinetics for adsorption with no axial dispersion and can be expressed as follows³⁴

$$\frac{C_t}{C_0} = \frac{1}{1 + \exp\left(\frac{k_{\text{Th}}q_0m}{Q} - k_{\text{Th}}C_0t\right)}$$

where *k*_{Th} is the Thomas rate constant (mL·mg⁻¹·min⁻¹), *q*₀ is the equilibrium adsorption capacity (mg·g⁻¹), *C*₀ and *C*_{*t*} are the Pb(II) concentration in the influent and that at time *t*, respectively (mg·L⁻¹), *m* is the weight of the adsorbent (g), *Q* is the flow rate (mL·min⁻¹), and *t* is the operation time (min).

The Thomas model could be expressed in the linear form as follows²⁴

$$\ln\left(\frac{C_0}{C_t} - 1\right) = \frac{k_{\text{Th}}q_0m}{Q} - k_{\text{Th}}C_0t$$

Based on the linear regression analysis using the above equation, the breakthrough curves and related parameters (*k*_{Th}, *q*₀, and *R*²) are obtained and presented in Figure 5a–c and Table 1, respectively. The Thomas model well described the breakthrough curves for all experimental conditions with high correlation coefficients in the range of 0.9512–0.9874. Additionally, the predicted adsorption capacity (*q*₀) values showed consistency with the experimental equilibrium column capacity (*q*_e) values (Table 1). In the case of different bed

heights, the breakthrough curves obtained from experiment data were not close to those predicted by the Thomas model as shown in Figure 5c. This might be due to the fact that the amount of the NaA zeolite phase in MKG@NaA was relatively low. In fact, the calculated amount of pure NaA zeolite was 1.62% in the bulk adsorbent, which caused the difference in breakthrough curve shape from experiment and simulated results.

As listed in Table 1 for the result obtained from the Thomas model, the adsorption capacity (*q*₀) was inversely proportional to the Thomas rate constant (*k*_{Th}). The *k*_{Th} value decreased with increasing weight of the adsorbent and influent concentration, while it increased with increasing inflow rate. The reason was that an increase in influent concentration increased the driving force for the mass transfer, leading to enhanced adsorption capacity. At the same time, it reduced the mass transfer rate due to the prolonged contact time between the solute and the adsorbent, leading to a decelerated Thomas rate constant. In addition, the increasing inflow rate reduced the interaction time between the Pb(II) ion and the adsorbent surface, leading to declined adsorption capacity. However, it increased the mass transfer rate, in turn increasing the Thomas constant. Conversely, as the weight of the adsorbent or the height of the column increased, the retention time of the solute in the column increased, which created higher adsorption capacity and lower Thomas rate constant.^{34,35}

2.5.2. Yoon–Nelson Model. The Yoon–Nelson model is a simple theoretical model that predicts the time required for 50% of adsorbent to reach the breakthrough point. It assumes that the adsorption probability for each adsorbed molecule has a decreasing rate, which is proportional to its adsorption and breakthrough probability on the adsorbent. The Yoon–Nelson model can be expressed as follows.³⁵

$$\frac{C_t}{C_0} = \frac{\exp(k_{\text{YN}}t - \tau k_{\text{YN}})}{1 + \exp(k_{\text{YN}}t - \tau k_{\text{YN}})}$$

where *k*_{YN} is the Yoon–Nelson rate constant (min⁻¹), τ is the time required for the 50% adsorbent to break through (min), *C*₀ and *C*_{*t*} are the Pb(II) concentration in the influent and that at time *t*, respectively (mg·L⁻¹), and *t* is the operation time (min).

The Yoon–Nelson model could be expressed in the linear form as follows²⁴

$$\ln\left(\frac{C_t}{C_0 - C_t}\right) = k_{YN}t - \tau k_{YN}$$

Derived from the linear regression analysis using the above equations to achieve the breakthrough curves and parameters (k_{YN} , τ , and R^2), the obtained results are presented in Figure 5a–c and Table 1, respectively. The Yoon–Nelson model generated the breakthrough curves that coincided with the one obtained from the Thomas model for all experimental conditions. The calculated result in Table 1 from the Yoon–Nelson model revealed that as the packing weights of the adsorbent increased, the 50% breakthrough time τ increased because the solution existed longer in the column and there was more contact time between the solute and the adsorbent. The obtained k_{YN} values increased and the 50% breakthrough time τ decreased with an increase in the initial concentration of the Pb(II) ion due to the bed column being saturated faster. It also showed that with increasing inflow rate, the values of k_{YN} increased and the values of τ decreased due to insufficient time for the Pb(II) ion to diffuse into the adsorbent.

2.5.3. BDST Model. Hutchins adapted the Adams–Bohart model to create the BDST model with the bed height (Z) and service time (t) in a linear relationship with each other. The BDST model assumes that the adsorption zone in the column has a constant movement rate and can be expressed as³⁶

$$t = \frac{N_0}{C_0 F} Z - \frac{1}{K_a C_0} \ln \ln \left(\frac{C_0}{C_t} - 1 \right) \quad (1)$$

where N_0 ($\text{mg}\cdot\text{L}^{-1}$) is the sorption capacity of the column, C_0 and C_t are the Pb(II) concentration in the influent and that at time t , respectively ($\text{mg}\cdot\text{L}^{-1}$), Z (m) is the height of the adsorbent in the column, F is the linear flow velocity ($\text{m}\cdot\text{h}^{-1}$), K_a is the rate constant ($\text{L}\cdot\text{mg}^{-1}\cdot\text{h}^{-1}$), and t is the breakthrough time (h). Equation 1 can be rewritten as follows

$$t = aZ - b \quad (2)$$

where:

$$a = \frac{N_0}{C_0 F}; \quad b = \frac{1}{K_a C_0} \ln \ln \left(\frac{C_0}{C_t} - 1 \right)$$

For a new operation condition with a given flow and concentration, eq 2 allowed for extrapolating new constants for the adsorption column.

From eqs 3 and 4, the new slope (a'), the new intercept (b'), and linear flow velocity (F') can be determined.

$$a' = a \frac{F}{F'} \quad (3)$$

$$b' = b \quad (4)$$

Or when the concentration of Pb(II) in new solution (C'_0) was known, from eqs 5 and 6, the new slope (a') and intercept (b') can be determined.

$$a' = a \frac{C_0}{C'_0} \quad (5)$$

$$b' = b \frac{C_0 \ln \ln(C'_0 - 1)}{C'_0 \ln \ln(C_0 - 1)} \quad (6)$$

In this work, the BDST model was applied, and the obtained result on the relation between the service time (t) and the bed

height (Z) for Pb(II) adsorption onto MKG@NaA is shown in Figure 6. It was observed that increasing the length of the bed

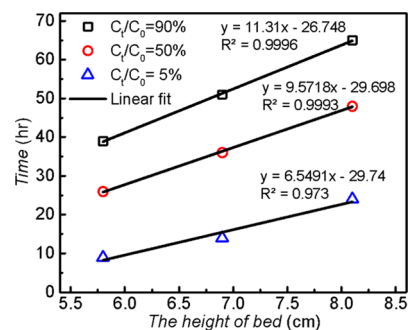


Figure 6. BDST model for 5, 50, and 90% breakthrough in the Pb(II) adsorption experiment using a fixed-bed column containing MKG@NaA with different bed heights, conducted at an inflow rate of $2 \text{ mL}\cdot\text{min}^{-1}$ and an initial solution concentration C_0 of $50 \text{ mg}\cdot\text{L}^{-1}$.

column would increase the contact time between the Pb(II) ions in solution and the adsorbent. As a result, the higher adsorption efficiency of Pb(II) ions and the longer breakthrough time were obtained. The model was applied for 5, 50, and 90% saturation of the column under a constant flow rate of $2 \text{ mL}\cdot\text{min}^{-1}$ and an influent Pb(II) concentration of 50 mg/L with good linearity ($R^2 > 0.9730$). From the slope (a) and intercept (b) parameters of the graphs, the values R^2 , N_0 , and K_a are calculated and presented in Table 2. The obtained result

Table 2. Calculated Parameters from the BDST Model for the Pb(II) Removal Using a Fixed-Bed Column Containing MKG@NaA, Conducted at an Inflow Rate of $2 \text{ mL}/\text{min}$ and an Initial Solution Concentration C_0 of 50 mg/L ^a

C_t/C_0	a (h/cm)	b (h)	N_0 (mg/L)	N'_0 (mg/g)	$K_a \times 10^3$ ($\text{L}/\text{mg}\cdot\text{h}$)	R^2
0.05	6.55	29.74	50,031	91.16	1.98	0.9730
0.5	9.57	29.70	73,123	133.24	0.00	0.9993
0.9	11.31	26.75	86,402	157.44	1.64	0.9996

^a C_0 , influent solution concentration (mg/L); C_t , effluent solution concentration at time t (mg/L); N_0 , sorption capacity in treated solution volume (mg/L); a , slope; b , intercept; N'_0 , adsorption capacity (mg/g); K_a , rate constant ($\text{L}/\text{mg}\cdot\text{h}$).

showed that when the C_t/C_0 ratio varied in values of 5, 50, and 90%, the column sorption capacity in the total treated solution volume (N_0) increased significantly from 50.03 to $86.40 \text{ g}\cdot\text{L}^{-1}$. In addition, the column adsorption capacity (N'_0) increased from 91.16 to $157.44 \text{ mg}\cdot\text{g}^{-1}$, whereas the K_a value decreased from 1.98×10^{-3} to $1.64 \times 10^{-3} \text{ L}\cdot\text{mg}^{-1}\cdot\text{h}^{-1}$. The obtained correlation coefficient (R^2) ranging from 0.9730 to 0.9996 proved that the BDST model can be used to predict the service time of the MKG@NaA material in the dynamic adsorption process, and the predicted column performance and adsorption efficiency under actual operating conditions can be calculated without further experimentation.^{35,36}

3. CONCLUSIONS

Overall, we report here a glue-free and simple procedure to synthesize NaA zeolite-coated metakaolin granules MKG@NaA by conventional hydrothermal treatment of metakaolin in sodium hydroxide solution without obtaining an additional precursor or zeolite seed crystal. The obtained MKG@NaA

material was used as an adsorbent in a fixed-bed column configuration for the dynamic adsorption of Pb(II) in solution by overcoming the aggregation and leakage of zeolite in powder form. The breakthrough point and saturation time of Pb(II) ion adsorption on MKG@NaA in the fixed-bed column varied depending on operation factors such as the influent Pb(II) ion concentration, fixed-bed height, and inflow rate. The experiment results were consistent with those obtained from applied calculated models such as the Thomas model, Yoon–Nelson model, and BDST model with relatively high linearity ($R^2 > 0.95$).

4. MATERIALS AND METHODS

4.1. Materials. The kaolin natural mineral (Lam Dong Province, Vietnam), NaOH (99%, Merck), NaCl (99.5%, Xilong Scientific), $\text{Pb}(\text{NO}_3)_2$ (>99%, Xilong Scientific), NaAlO_2 (Alfa Aesar), sodium orthosilicate (Na_4SiO_4 , Alfa Aesar), and HNO_3 (65% Sigma-Aldrich) were used as received without further purification.

4.2. Preparation of NaA Zeolite-Coated Metakaolin Granules (MKG@NaA). Kaolinite clay in semisolid form was first dried and ground. The kaolinite granules with the size of about 2 mm were collected by sieving through a 10-mesh sieve. Prepared kaolinite was calcined at the temperature of 500 °C for 3 h, resulting in a more active metakaolin form.

The cubic-shaped NaA zeolite crystals with an average size of $1.4 \mu\text{m}^3$ coated on granular metakaolin were synthesized by conventional hydrothermal reaction using metakaolin granules (MKG) and sodium hydroxide aqueous solution. For a typical experiment, 2.056 g of MKG was mixed with 8.0 mL of 2.33 M NaOH solution in a plastic beaker. The beaker was covered with a plastic grab and the mixture was aged for 24 h with gentle stirring at a speed of 200 rpm at room temperature. After aging time, the mixture was transferred into a Teflon-lined autoclave and placed in a convection oven. The hydrothermal reaction was carried out at a temperature of 100 °C for 24 h. After the hydrothermal reaction, the autoclave was cooled down by tap water. The MKG@NaA product was collected, washed with a copious amount of deionized water (DIW) until neutral pH, and soaked in 10 mL of 100 mg/L NaCl solution for 8 h at room temperature to convert all exchangeable sites to Na^+ form and to eliminate the precipitation of heavy metal ions in later studies. Finally, the MKG@NaA product was collected and washed three times with distilled water. The final product was dried at 105 °C for 8 h.

4.3. Fixed-Bed Column Adsorption Experiments. The batch adsorption of heavy metal ions using a batch reactor and NaA zeolite powder as the adsorbent was first conducted to study the highest adsorption capacity of NaA zeolite to heavy metal ions. The experiments were carried out by adding 100 mg of NaA zeolite powder to 150 mL of solution containing single metal ions including Pb(II), Cd(II), Co(II), and Ni(II) with designed concentration. After a period of experiment, 2 mL of solution with zeolite was collected. Zeolite was separated by centrifugation, and the remaining concentration of metal ions in solution was measured.

The adsorption of lead Pb(II) in aqueous solution using MKG@NaA was carried out in a fixed-bed column with a laboratory scale using a Pyrex glass column with the length and inner diameter of 25 and 1 cm, respectively. A layer of 1 cm-thick glass wool was fitted at the bottom of the column to keep MKG@NaA from spilling out. The adsorbent with the

designed amount was packed into the column and washed with DIW before conducting the adsorption experiment. The study parameters including the input flow rate of Pb(II) metal ion solution, the height of the adsorbent bed layer, and the initial concentration of Pb(II) ion solution were studied. The flow rate of Pb(II) metal ion solution in values of 2.0, 2.5, and 3.0 mL/min was varied by a peristaltic pump. The height of the adsorbent bed layer was varied in values of 5.8, 6.9, and 8.1 cm corresponding to 2.5, 3.0, and 3.5 g of MKG@NaA material, respectively. The initial concentration of Pb(II) ion solution was varied in values of 50, 80, and 100 mg/L. After the designed experiment period, the effluent solution was collected, and the remaining Pb(II) ion concentration was measured.

The breakthrough curve represents the efficiency of a fixed-bed column, which is expressed by a graph of C_t/C_0 versus adsorption time for a given bed height (where C_0 and C_t are the effluent Pb(II) concentration and the influent Pb(II) concentration at time t , respectively). The breakthrough curve indicates the operation time until the column is saturated, wherein its shape characterizes the behavior and the dynamic response of a fixed-bed column. The working limit of the column in Pb(II) ion removal is determined by column adsorption capacity at the breakpoint value of 0.05. At this breakpoint, the Pb(II) ion concentration (C_t) in the effluent solution in the output was 5% compared to that in the input flow (C_0). The adsorption behavior of the column was obtained from experiment data and calculated from breakthrough curves as follows.

The treated solution volume V_t was calculated from the flow rate of treated solution, Q ($\text{mL}\cdot\text{min}^{-1}$), and the operating time of the fixed-bed column, t_e (min), as the following equation:³²

$$V_t = Q \times t_e$$

The fixed-bed capacity q_{total} (mg) can be obtained from the equation:

$$q_{\text{total}} = \frac{Q \times A}{1000} = \frac{Q}{1000} \int_{t=0}^{t=t_e} (C_0 - C_t) \times dt$$

where t_s (min) represents the saturation time, C_0 ($\text{mg}\cdot\text{L}^{-1}$) is the initial concentration of lead ions, C_t is the concentration of lead ions in aqueous solution after adsorption time “ t ”, and A is the area under the breakthrough curve.

The equilibrium column capacity (q_e , $\text{mg}\cdot\text{g}^{-1}$) is calculated as follows, with m (g) being the amount of the adsorbent in the column.

$$q_e = \frac{q_{\text{total}}}{m}$$

The total amount of lead ions (m_{total} , g) adsorbed to the column can be calculated from the following equation:

$$m_{\text{total}} = \frac{C_0 \times Q \times t_s}{1000}$$

The total removal percentage (R_{total}) of lead ions for the fixed-bed column at saturation can be calculated as follows:

$$R_{\text{total}}(\%) = \frac{q_{\text{total}}}{m_{\text{total}}}$$

4.4. Analytical Methods. Scanning electron microscopy (SEM) measurement was conducted using a scanning electron microscope JSM-6400 operating at an acceleration voltage of 5

kV. Powder X-ray diffraction (XRD) patterns were obtained from a Bruker D8 Advance powder X-ray diffractometer performing at 40 kV and 40 mA with Cu K α radiation. Flame atomic absorption spectrophotometry (FAAS) was performed using a Shimadzu AA-6300 (Japan) for the measurement of Pb(II) ion concentration in solution. Energy dispersive X-ray (EDX) measurements were performed using a Hitachi FESEM S4800 and Horiba EDX H-7593.

AUTHOR INFORMATION

Corresponding Authors

Tung Cao-Thanh Pham – Vietnam Academy of Science and Technology, Institute of Chemical Technology, Ho Chi Minh City 71515, Vietnam; orcid.org/0000-0002-4631-481X; Email: pcttung@ict.vast.vn

Thanh Tu Le – University of Science, Ho Chi Minh City 72711, Vietnam; Vietnam National University, Ho Chi Minh City 72711, Vietnam; Email: letuthanh@hcmus.edu.vn

Authors

Hieu Nguyen Phuoc – University of Science, Ho Chi Minh City 72711, Vietnam; Vietnam National University, Ho Chi Minh City 72711, Vietnam

Quang Thanh Le – Vietnam Academy of Science and Technology, Institute of Chemical Technology, Ho Chi Minh City 71515, Vietnam

Complete contact information is available at:

<https://pubs.acs.org/10.1021/acsoomega.1c02658>

Notes

The authors declare no competing financial interest.

ACKNOWLEDGMENTS

This work was funded by the support from Vietnam National University, Ho Chi Minh City, Vietnam, for project code no. C2018-18-23. We would like to thank Associate Professor Nguyen Van Dong from the Faculty of Chemistry, University of Science, VNU-HCMC, for supporting the heavy metal ion measurement.

REFERENCES

- (1) Raúl, F. Lobo. *Handbook of Zeolite Science and Technology*; S. Auerbach, K.; Carrado, P. D., Ed.; Marcel Dekker: New York, 2003.
- (2) Datta, S. J.; Moon, W. K.; Choi, D. Y.; Hwang, I. C.; Yoon, K. B. A Novel Vanadosilicate with Hexadeca-Coordinated Cs⁺ Ions as a Highly Effective Cs⁺ Remover. *Angew. Chem., Int. Ed.* **2014**, *53*, 7203–7208.
- (3) Datta, S. J.; Oleynikov, P.; Moon, W. K.; Ma, Y.; Mayoral, A.; Kim, H.; Dejoie, C.; Song, M. K.; Terasaki, O.; Yoon, K. B. Removal of ⁹⁰Sr from Highly Na⁺-Rich Liquid Nuclear Waste with a Layered Vanadosilicate. *Energy Environ. Sci.* **2019**, *12*, 1857–1865.
- (4) Chapman, W. K.; Chupas, J. P.; Nenoff, T. M. Radioactive Iodine Capture in Silver-Containing Mordenites through Nanoscale Silver Iodide Formation. *J. Am. Chem. Soc.* **2010**, *132*, 8897–8899.
- (5) Pham, C. T. T.; Docao, S.; Hwang, I. C.; Song, M. K.; Moon, D.; Oleynikov, P.; Yoon, K. B. Capture of Iodine and Organic Iodides Using Silica Zeolites and the Semiconductor Behaviour of Iodine in a Silica Zeolite. *Energy Environ. Sci.* **2016**, *9*, 1050–1062.
- (6) Collins, F.; Rozhkovskaya, A.; Outram, J. G.; Millar, G. J. A Critical Review of Waste Resources, Synthesis, and Applications for Zeolite LTA. *Microporous Mesoporous Mater.* **2020**, *291*, 109667.
- (7) Jawor, A.; Hoek, E. M. V. Removing Cadmium Ions from Water via Nanoparticle-Enhanced Ultrafiltration. *Environ. Sci. Technol.* **2010**, *44*, 2570–2576.

- (8) El-Kamash, A. M. Evaluation of Zeolite A for the Sorptive Removal of Cs⁺ and Sr²⁺ Ions from Aqueous Solutions Using Batch and Fixed Bed Column Operations. *J. Hazard. Mater.* **2008**, *151*, 432–445.

- (9) Xie, W. M.; Zhou, F. P.; Bi, X. L.; Chen, D. D.; Li, J.; Sun, S. Y.; Liu, J. Y.; Chen, X. Q. Accelerated Crystallization of Magnetic 4A-Zeolite Synthesized from Red Mud for Application in Removal of Mixed Heavy Metal Ions. *J. Hazard. Mater.* **2018**, *358*, 441–449.

- (10) El-Kamash, A. M.; Zaki, A. A.; El Geleel, M. A. Modeling Batch Kinetics and Thermodynamics of Zinc and Cadmium Ions Removal from Waste Solutions Using Synthetic Zeolite A. *J. Hazard. Mater.* **2005**, *127*, 211–220.

- (11) Ibrahim, H. S.; Jamil, T. S.; Hegazy, E. Z. Application of Zeolite Prepared from Egyptian Kaolin for the Removal of Heavy Metals: II. Isotherm Models. *J. Hazard. Mater.* **2010**, *182*, 842–847.

- (12) Izidoro, J. d. C.; Fungaro, D. A.; Abbott, J. E.; Wang, S. Synthesis of Zeolites X and A from Fly Ashes for Cadmium and Zinc Removal from Aqueous Solutions in Single and Binary Ion Systems. *Fuel* **2013**, *103*, 827–834.

- (13) Holmes, S. M.; Alomair, A. A.; Kovo, A. S. The Direct Synthesis of Pure Zeolite-A Using 'Virgin' Kaolin. *RSC Adv.* **2012**, *2*, 11491–11494.

- (14) Fardjaoui, N.-E.-H.; El Berrichi, F. Z.; Ayari, F. Kaolin-Issued Zeolite A as Efficient Adsorbent for Bezanyl Yellow and Nylomine Green Anionic Dyes. *Microporous Mesoporous Mater.* **2017**, *243*, 91–101.

- (15) Johnson, E. B. G.; Arshad, S. E. Hydrothermally Synthesized Zeolites Based on Kaolinite: A Review. *Appl. Clay Sci.* **2014**, *97–98*, 215–221.

- (16) Abdullahi, T.; Harun, Z.; Othman, M. H. D. A Review on Sustainable Synthesis of Zeolite from Kaolinite Resources via Hydrothermal Process. *Adv. Powder Technol.* **2017**, *28*, 1827–1840.

- (17) Wang, J.-Q.; Huang, Y.-X.; Pan, Y.; Mi, J.-X. Hydrothermal Synthesis of High Purity Zeolite A from Natural Kaolin without Calcination. *Microporous Mesoporous Mater.* **2014**, *199*, 50–56.

- (18) Wang, J. Q.; Huang, Y. X.; Pan, Y.; Mi, J. X. New Hydrothermal Route for the Synthesis of High Purity Nanoparticles of Zeolite γ from Kaolin and Quartz. *Microporous Mesoporous Mater.* **2016**, *232*, 77–85.

- (19) Lin, L.; Wang, A.; Dong, M.; Zhang, Y.; He, B.; Li, H. Sulfur Removal from Fuel Using Zeolites/Polyimide Mixed Matrix Membrane Adsorbents. *J. Hazard. Mater.* **2012**, *203–204*, 204–212.

- (20) Ulusoy, U.; Şimşek, S. Lead Removal by Polyacrylamide-Bentonite and Zeolite Composites: Effect of Phytic Acid Immobilization. *J. Hazard. Mater.* **2005**, *127*, 163–171.

- (21) Liu, Y.; Yang, X.; Yan, C.; Wang, H.; Zhou, S. Solvent-Free Synthesis of Zeolite LTA Monolith with Hierarchically Porous Structure from Metakaolin. *Mater. Lett.* **2019**, *248*, 28–31.

- (22) Bessa, R. d. A.; Costa, L. d. S.; Oliveira, C. P.; Bohn, F.; do Nascimento, R. F.; Sasaki, J. M.; Loiola, A. R. Kaolin-Based Magnetic Zeolites A and P as Water Softeners. *Microporous Mesoporous Mater.* **2017**, *245*, 64–72.

- (23) Mokgehle, T. M.; Gitari, W. M.; Tavengwa, N. T. Synthesis of Di-Carboxylic Acid Functionalized Zeolites from Coal Fly Ash for Cd(II) Removal from Acid Mine Drainage Using Column Studies Approach. *J. Environ. Chem. Eng.* **2019**, *7*, 103473.

- (24) Dong, Y.; Lin, H. Competitive Adsorption of Pb(II) and Zn(II) from Aqueous Solution by Modified Beer Lees in a Fixed Bed Column. *Process Saf. Environ. Prot.* **2017**, *111*, 263–269.

- (25) Yanyan, L.; Kurniawan, T. A.; Zhu, M.; Ouyang, T.; Avtar, R.; Dzafan Othman, M. H.; Mohammad, B. T.; Albadarin, A. B. Removal of Acetaminophen from Synthetic Wastewater in a Fixed-Bed Column Adsorption Using Low-Cost Coconut Shell Waste Pretreated with NaOH, HNO₃, Ozone, and/or Chitosan. *J. Environ. Manage.* **2018**, *226*, 365–376.

- (26) Fu, F.; Wang, Q. Removal of Heavy Metal Ions from Wastewaters: A Review. *J. Environ. Manage.* **2011**, *92*, 407–418.

- (27) Sprynskyy, M.; Buszewski, B.; Terzyk, A. P.; Namięśnik, J. Study of the Selection Mechanism of Heavy Metal (Pb²⁺, Cu²⁺, Ni²⁺,

and Cd²⁺) Adsorption on Clinoptilolite. *J. Colloid Interface Sci.* **2006**, *304*, 21–28.

(28) Alswata, A. A.; Ahmad, M. B.; Al-Hada, N. M.; Kamari, H. M.; Hussein, M. Z. B.; Ibrahim, N. A. Preparation of Zeolite/Zinc Oxide Nanocomposites for Toxic Metals Removal from Water. *Results Phys.* **2017**, *7*, 723–731.

(29) Azimi, A.; Azari, A.; Rezakazemi, M.; Ansarpour, M. Removal of Heavy Metals from Industrial Wastewaters: A Review. *ChemBioEng Rev.* **2017**, *4*, 37–59.

(30) Ren, Y.; Yan, N.; Wen, Q.; Fan, Z.; Wei, T.; Zhang, M.; Ma, J. Graphene/ δ -MnO₂ Composite as Adsorbent for the Removal of Nickel Ions from Wastewater. *Chem. Eng. J.* **2011**, *175*, 1–7.

(31) Anari-Anaraki, M.; Nezamzadeh-Ejhi, A. Modification of an Iranian Clinoptilolite Nano-Particles by Hexadecyltrimethyl Ammonium Cationic Surfactant and Dithizone for Removal of Pb(II) from Aqueous Solution. *J. Colloid Interface Sci.* **2015**, *440*, 272–281.

(32) Qu, J.; Song, T.; Liang, J.; Bai, X.; Li, Y.; Wei, Y.; Huang, S.; Dong, L.; Jin, Y. Adsorption of Lead (II) from Aqueous Solution by Modified Auricularia Matrix Waste: A Fixed-Bed Column Study. *Ecotoxicol. Environ. Saf.* **2019**, *169*, 722–729.

(33) Gouran-Orimi, R.; Mirzayi, B.; Nematollahzadeh, A.; Tardast, A. Competitive Adsorption of Nitrate in Fixed-Bed Column Packed with Bio-Inspired Polydopamine Coated Zeolite. *J. Environ. Chem. Eng.* **2018**, *6*, 2232–2240.

(34) Han, R.; Wang, Y.; Zhao, X.; Wang, Y.; Xie, F.; Cheng, J.; Tang, M. Adsorption of Methylene Blue by Phoenix Tree Leaf Powder in a Fixed-Bed Column: Experiments and Prediction of Breakthrough Curves. *Desalination* **2009**, *245*, 284–297.

(35) Vijayaraghavan, K.; Prabu, D. Potential of Sargassum Wightii Biomass for Copper(II) Removal from Aqueous Solutions: Application of Different Mathematical Models to Batch and Continuous Biosorption Data. *J. Hazard. Mater.* **2006**, *137*, 558–564.

(36) Zhang, Y.; Jin, F.; Shen, Z.; Wang, F.; Lynch, R.; Al-Tabbaa, A. Adsorption of Methyl Tert-Butyl Ether (MTBE) onto ZSM-5 Zeolite: Fixed-Bed Column Tests, Breakthrough Curve Modelling and Regeneration. *Chemosphere* **2019**, *220*, 422–431.